Lithium Metal Batteries | Hot Paper

How to cite:
International Edition: doi.org/10.1002/anie.202017063
German Edition: doi.org/10.1002/ange.202017063

Li-Rich $Li_2[Ni_{0.8}Co_{0.1}Mn_{0.1}]O_2$ for Anode-Free Lithium Metal Batteries

Liangdong Lin, Kun Qin, Qinghua Zhang, Lin Gu, Liumin Suo, Yong-sheng Hu, Hong Li, Xuejie Huang, and Liquan Chen*

Abstract: *Anode-free lithium metal batteries can maximize the energy density at the cell level. However, without the Li compensation from the anode side, it faces much more challenging to achieve a long cycling life with a competitive energy density than Li metal-based batteries. Here, we prolong the lifespan of an anode-free Li metal battery by introducing Li-rich $Li_2[Ni_{0.8}Co_{0.1}Mn_{0.1}]O_2$ into the cathode as a Li-ions extender. The $Li_2[Ni_{0.8}Co_{0.1}Mn_{0.1}]O_2$ can release a large amount of Li-ions during the first charging process to supplement the Li loss in the anode, then convert into NCM811, thus extending the lifespan of the battery without the introduction of inactive elements. By the benefit of Li-rich cathode and high reversibility of Li metal on Cu foil, the anode-free pouch cells enable to achieve 447 Wh kg^{-1} energy density and 84% capacity retention after 100 cycles in the condition of limited electrolyte addition (E/C ratio of 2 g Ah^{-1}).*

Introduction

Lithium-ion batteries (LIBs) have dominated the consumer electronics market and continually penetrating the electric vehicle and electric energy storage markets.[1] However, the rock-chair configuration of the traditional Li-ion chemistry restricts the energy density of LIBs less than 300 Wh kg^{-1}, which is unsatisfactory in those emerging application scenarios.[1c,2] Under the circumstances, Li metal-based batteries (LMBs) are reconsidered as the next-generation beyond Li-ion batteries.[3] Since Li anode processes the reversibly electrochemical plating/stripping and Li contained cathode enables to provide Li resource; theoretically, the anode free is feasible for LMBs that is called "anode-free lithium metal batteries (AF-LMBs).[4] AF-LMBs are regarded as the ultimate choice for Li metal batteries with a very high theoretical energy density. Compared to the traditional LMBs, the removal of the anode materials would maximize the energy density of LMBs exceeding 400 Wh kg^{-1} at the cell level.[5] Among various cathode materials (Table S1),[6] $Li[Ni_{0.8}Co_{0.1}Mn_{0.1}]O_2$ (NCM811) shows the most balanced properties with high energy density and cycling stability,[7] which is perfect for AF-LMBs.[8]

Despite that, it is also definitely more challenging for AF-LMBs to achieve a long cycling life without Li compensation from the anode side than traditional LMBs. The lithium metal anode (LMA) usually suffer from the low Coulombic efficiency (CE) and the fast capacity fading resulting from seriously the virtually infinite volume change, potential dendrite growth (dead Li generation) during Li plating (stripping) and the continual side-reaction consuming by the formation of non-robust solid electrolyte interphase (SEI).[3] Recently, the CE of the state-of-art LMAs has been improved significantly above 99.5% by developing functional electrolytes,[8b,9] interface engineering,[10] and using robust hosts;[11] however, it is still far from the absolute AF-LMBs' requirement of $>99.98\%$, assuming that the cycle life of the LMBs achieves >1000 cycles with the capacity retention of $>80\%$. Meanwhile, as the reported AF-LMBs using NCM or NCA as a cathode summarized in Table S2, so far, most of their areal capacities are less than 3 mAh cm^{-2} that limited the energy density at the cell level below 300 Wh kg^{-1}, and almost all these AF-LMBs except Dahn's and Cui's works are evaluated in coin cells.[4b,8c,12] Thus, it is indeed a critical challenge for AF-LMBs to lasting cycling life with above 300 Wh kg^{-1} at the full cell level.

Herein, Li-rich $Li_2[Ni_{0.8}Co_{0.1}Mn_{0.1}]O_2$ (short for Li_2NCM811) material with $P\bar{3}m1$ structure has been partly applied into the cathode for AF-LMB to extend its lifespan, like a disposable fuel tank for a space shuttle. When comparing with conventional $Li[Ni_{0.8}Co_{0.1}Mn_{0.1}]O_2$ (NCM811) material,[13] nearly twice of the Li resources are stored in the Li layer of Li_2NCM811 without affecting the structural stability of the transition metal layer, as illustrated in Figure 1a. The Li_2NCM811 can be reversibly converted into conventional NCM811 by de-intercalation of excess Li from the Li layer during the first charging process, and the excess Li resources will be temporarily stored in the anode (Figure 1a). After that, it will function as a conventional NCM811 cathode and work steadily in the future cycles. Besides, unlike pre-lithiation additives,[14] the Li resources

[*] Dr. L. Lin, K. Qin, Prof. L. Suo, Prof. Y. Hu, Prof. H. Li, Prof. X. Huang, Prof. L. Chen
Beijing Advanced Innovation Center for Materials Genome Engineering, Key Laboratory for Renewable Energy, Beijing Key Laboratory for New Energy Material and Devices, Beijing National Laboratory for Condensed Matter Physics, Institute of Physics, Chinese Academy of Science
Beijing, 100190 (China)
E-mail: suoliumin@iphy.ac.cn
Dr. L. Lin, K. Qin, Prof. L. Suo
Center of Materials Science and Optoelectronics Engineering, University of Chinese Academy of Sciences
Beijing, 100049 (China)
Prof. Q. Zhang, Prof. L. Gu, Prof. L. Suo
Yangtze River Delta Physics Research Center Co. Ltd
Liyang, 213300 (China)
Prof. Q. Zhang, Prof. L. Gu
Beijing National Laboratory for Condensed Matter Physics, Institute of Physics, Chinese Academy of Science
Beijing, 100190 (China)
Supporting information and the ORCID identification number(s) for the author(s) of this article can be found under: https://doi.org/10.1002/anie.202017063.

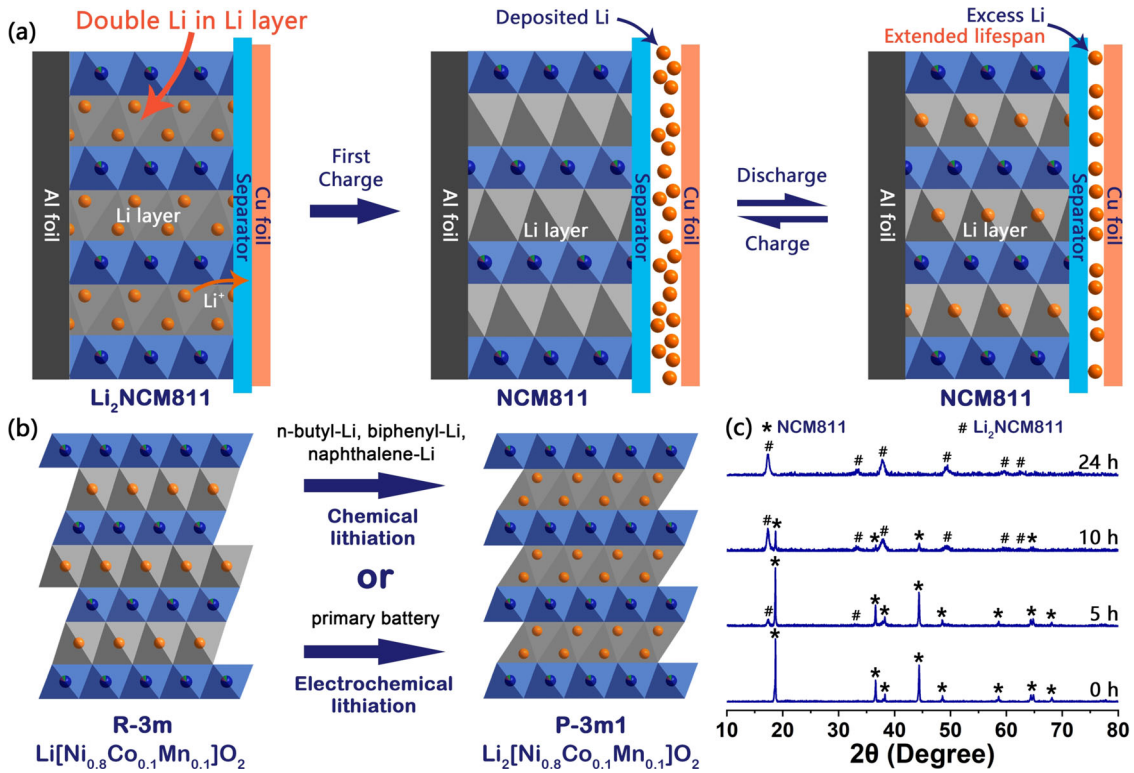

Figure 1. The concept of $Li_2[Ni_{0.8}Co_{0.1}Mn_{0.1}]O_2$ (Li_2NCM811) based anode-free Li metal batteries. a) Scheme of Li_2NCM811 extending the lifespan of AF-LMB. b) The illustration of Li_2NCM811 synthesized by chemical lithiation or electrochemical lithiation. c) XRD patterns of NCM811 react with n-butyl Li for different hours.

stored in Li_2NCM811 can be 100% converted into active Li, without the introduction of additional mass brought up by other inactive elements, thus improving the lifespan of AF-LMB without sacrificing its energy density. More importantly, the operation of such AF-LMB during storage or transport before the first charge is more convenient than that of Li-containing LMBs without highly reactive metallic Li. All these factors make this concept very attractive for the development of long-life and high energy density LMBs.

It is worth noting that the $P\bar{3}m1$ structure is not the ground state of $Li_2[Ni_{0.8}Co_{0.1}Mn_{0.1}]O_2$ and hardly synthesize directly by solid-state reaction.[15] However, it can be obtained by the over-lithiation of NCM811 with the $R\bar{3}m$ structure,[16] including chemical lithiation and electrochemical lithiation (Figure 1b,c, and S1–S4). For example, Li_2NCM811 can be obtained by the reaction of n-butyl Li with NCM811. With the increase of reaction time, NCM811 can be completely lithiated, confirmed by the disappearance of NCM811 reflections, as shown in Figure 1c. Notably, only partly lithiated NCM811 are used in cell fabrication, as explained in Figure S5. The lithiated NCM811, composed of NCM811 core and Li_2NCM811 shell, is named $Li_{1+x}[Ni_{0.8}Co_{0.1}Mn_{0.1}]O_2$ (short for Li_{1+x}NCM811, $0<x\leq1$) based on its chemical composition as determined by ICP (Table S3). For example, NCM811 with a lithiation degree of 37% is named $Li_{1.37}[Ni_{0.8}Co_{0.1}Mn_{0.1}]O_2$ ($Li_{1.37}$NCM811). Using this Li_{1+x}NCM811 as a cathode, the anode-free pouch cell we assembled with high cathode mass loading (25 mg cm^{-2}) and limited electrolyte addition (E/C ratio of 2 g Ah^{-1}) shows a high capacity retention of 84% after 100 cycles.

Results and Discussion

From the voltage profiles of NCM811 half-cells with different cut-off voltages (Figure S6), a new reversible plateau appears at 1.8 V, confirming the reversible conversion between Li_2NCM811 and NCM811. Furthermore, in situ X-ray Diffraction (XRD) was performed to observe the complete discharge and charge process of NCM811 visually. Before the in situ XRD measurement, the in situ cell was charged to 4.3 V, and then constant voltage was charged until the current dropped below 0.02 C (1 C = 200 mA g^{-1}). Subsequently, the in situ XRD test was carried out with the following first discharge process to 1.6 V and re-charge to 4.3 V under a current density of 0.1C. Figure 2a shows contour plots illustrating the evolution of the NCM811 reflections whose corresponding XRD patterns in Figure S7. At first glance, all Bragg reflections of NCM811 show quite good reversibility. Rietveld refinement of the XRD pattern discharged to 2.6 V confirmed the sample to be of the layered R-3 m type NCM811 (Figure 2b), in agreement with literature reports.[13a,c] Notably, the characteristic (002), (100), and (014) reflections of $P\bar{3}m1$ type Li_2NCM811 also gradually appear as the over-discharge progressed. The (002) plane of Li_2NCM811 originates from the (003) plane of NCM811, proving that Li ions can continue to intercalate into the Li layer of NCM811 while maintaining the layered structure. Through the Rietveld refinement of the XRD pattern discharged to 1.6 V (Figure 2c), the coexist of $R\bar{3}m$ NCM811 and $P\bar{3}m1$ Li_2NCM811 can be confirmed. And the d-spacing of the NCM811 (003) plane has increased from 0.473 nm to

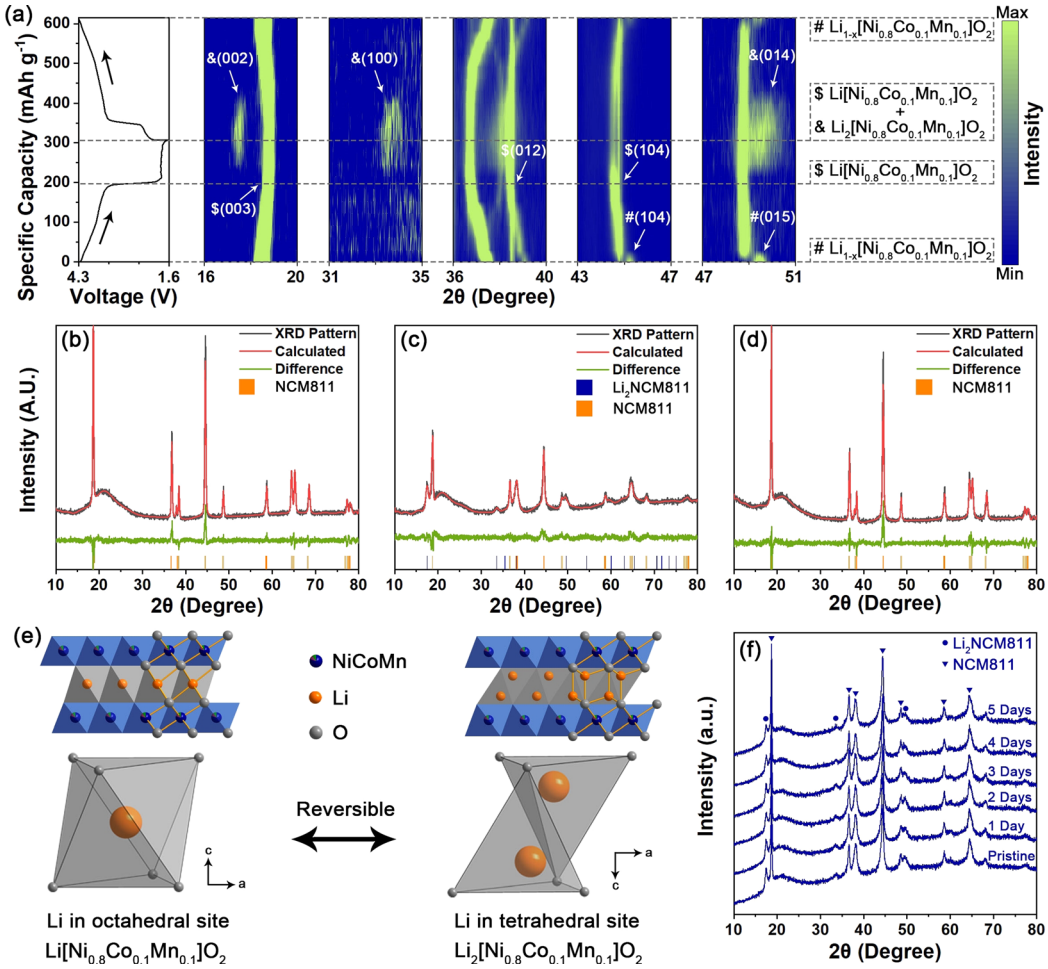

Figure 2. The evaluation of the reversible phase transition between NCM811 and Li_2NCM811. a) Contour plot of in situ XRD patterns of an NCM811 half-cell along with corresponding voltage profiles. XRD patterns, along with corresponding Rietveld refinements of NCM811 cathodes (b) discharged to 2.6 V, c) discharged to 1.6 V, and d) charged back to 3.6 V. e) Crystal structures of NCM811 and Li_2NCM811 along with corresponding Li occupations. f) The chemical stability of lithiated NCM811 cathode in air with a humidity of 15%.

0.506 nm to form the (002) plane of Li_2NCM811. Then, the (002), (100), and (014) reflections of Li_2NCM811 disappear during the charging process, indicating the reversibility of this over-lithiation reaction. Rietveld refinement of the XRD pattern charged back to 3.6 V confirmed the disappearance of $P\bar{3}m1$ Li_2NCM811 (Figure 2d). The intensity of NCM811 reflections also becomes stronger again, indicating that $P\bar{3}m1$ Li_2NCM811 converted back to $R\bar{3}m$ NCM811. Similar lithiation reaction of $LiNiO_2$ to form $P\bar{3}m1$ structure Li_2NiO_2 has been reported by Dahn et al.[16]

The over-lithiation process will drive the octahedral Li-ions into tetrahedral sites, as illustrated in Figure 2e. However, the Li-ion conduction in the Li layer of NCM811 occurs from one octahedral site to another via a neighboring tetrahedral void that shares faces with three octahedral within the Li layer as it offers the lowest energy barrier.[15] The occupation of all tetrahedral sites in Li_2NCM811 certainly blocks the diffusion pathways towards the bulk resulting in an apparent overpotential (Figure S8 and S9). Thus, it might not be suitable for energy storage limited by the show kinetic, and the relatively low working potential < 2.5 V regarded as the invalid capacity in full cell. However, it is an ideal Li supplementation. After completing its mission for Li supplementation, Li_2NCM811 can continue to participate in cell cycling function as an NCM811 cathode. Notably, the chemical stability of Li_2NCM811 stored in the air with a humidity of 15% is also satisfactory (Figure 2f), although slight oxidation occurs at the surface (Figure S10). Even exposed to air with a humidity of 15% for five days, the reflections of Li_2NCM811 can still be observed from the XRD pattern. This also makes Li_2NCM811 possibly applied in other LIBs to compensate for the Li loss resulting from low CE.

The two-phase distribution and crystal structure of lithiated NCM811 are further investigated by Spherical Aberration Corrected Transmission Electron Microscope (ABF-STEM) combining with Electron Energy Loss Spectroscopy (EELS). Figure 3a shows the EELS spectra of Ni, whose corresponding spectra collection sites in Figure S11–S13. It observed an evident shift of Ni energy loss peak from 858 to 857 eV in the lithiated NCM811, indicating that the continued insertion of Li ions reduced the valence of Ni from 3^+ to 2^+.[17] As the EELS linear profile of a lithiated cathode particle shown in Figures 3b and c, the outer layer of the cathode particle exhibits two valent Ni and with the scan

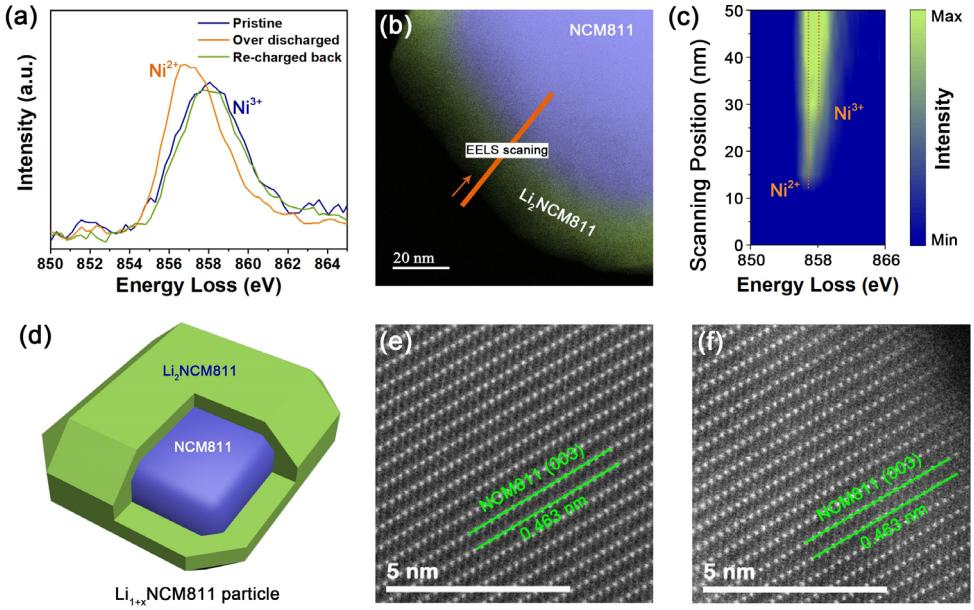

Figure 3. The confirmation of the lithiated NCM811 composite structure. a) EELS spectra of pristine NCM811, over-discharged NCM811, and re-charged back NCM811 cathode. b) STEM image of an lithiated NCM811 particle over-discharge to 1.6 V along with the path of EELS liner scan. c) Contour plot of EELS spectra obtained from the EELS linear scan of an over-discharged NCM811 particle. d) Scheme of a lithiated $Li_{1+x}NCM811$ particle over-discharge to 1.6 V. e) HAADF-STEM image of an NCM811 particle. f) HAADF-STEM image of an NCM811 particle first discharge to 1.6 V and then charge back to 3.6 V.

progressed deep into the inner particle, the energy loss peak of Ni broadened toward the high valence, indicating the coexistence of 2^+ and 3^+ Ni. It reveals the formation of $Li_2NCM811$ locals on the surface of the lithiated NCM811 particles and forms the core–shell structure of NCM811-$Li_2NCM811$, as illustrated in Figure 3 d. The possible reason is that the strong electrostatic repulsion between the tetrahedral Li-ions in $P\bar{3}m1$ $Li_2NCM811$ mentioned above might result in the blockage of Li migration channels, and the NCM811 deep inside the particle cannot be further lithiated. Meanwhile, as the Figure 3 e and f show, the cycled NCM811 after over-discharge to 1.6 V still maintain the identified (003) plane of NCM811 intuitively, double confirming the reversible conversion between $Li_2NCM811$ and NCM811.

Considering that it has approximately 6.8 % volume expansion from NCM811 to $Li_2NCM811$, the electrochemical performance of $Li_{1+x}NCM811$ was evaluated in the half-cells by the electrochemical controlling ratio of $Li_2NCM811$ to NCM811 (Figure 4). The preparation and cycling stability of $Li_{1+x}NCM811$ with different over-lithiation degrees are discussed in Figure S14 and S15, whose corresponding initial capacities and capacity retentions after 100 cycles are summarized in Figure 4 a. It manifests that a higher lithiated degree indeed increases the initial discharge capacity, but, with the continual increment of over-lithiation, the capacity retention began to contaminate once the value exceeds above $\approx$25 mol %. It possibly results from the low binder content in the high loading cathode (only 2 wt %) is susceptible to volume expansion. However, in the following experiment, the mol percentage of $Li_2NCM811$ in the cathode is controlled at less than 40 mol %.

Figure 4 b shows the electrochemical over-lithiated voltage profiles of $Li_{1.2}NCM811$. The specific discharge capacity

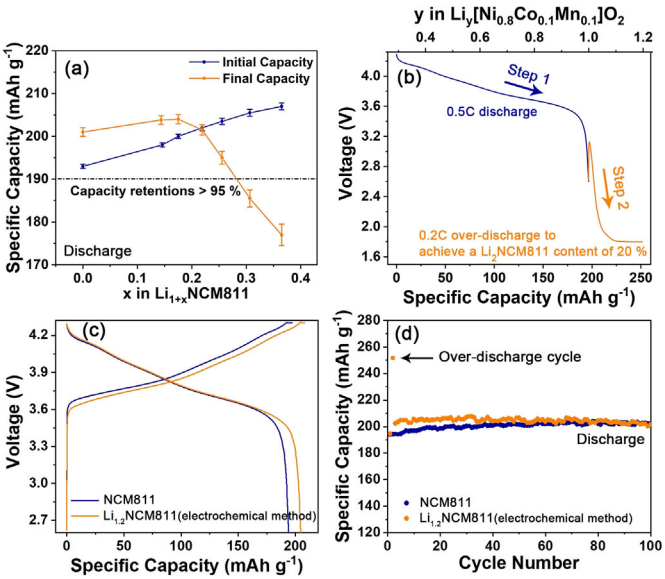

Figure 4. The electrochemical performance of $Li_{1+x}NCM811$ cathode. a) Initial capacities and final capacities (bars donate SD) after 100 cycles of $Li_{1+x}NCM811$ half-cells with different content of $Li_2NCM811$. b) Voltage profiles of an NCM811 half-cell discharge to 2.6 V and then over-discharge to achieve a $Li_2NCM811$ content of 20 %. c) Voltage profiles and d) cycling performances of NCM811 half-cell and $Li_{1.2}NCM811$ half-cell. ($Li_{1.2}NCM811$ was lithiated by over-discharge of a half-cell.)

is 196.50 mAh g^{-1} into 2.6 V at 0.5 C, then the continued over-discharge until the specific capacity increased by 55.07 mAh g^{-1} at 0.2 C (20.45 % of the theoretical capacity). The electrochemical performances of the $Li_{1.2}NCM811$ cathode were further compared with the NCM811 cathode

(Figure 4c and 4d). Surprisingly, the $Li_{1.2}$NCM811 cell delivers a discharge capacity of 204.78 mAh g^{-1} (4.3–2.6 V), apparently outperforming the NCM811 cathode (194.06 mAh g^{-1}, Figure 4c) consistent with the discovery in the NCM811 cathode, whose capacity also increased after electrochemical over-lithiation (Figure S16). Meanwhile, $Li_{1.2}$NCM811 half-cells exhibit excellent cycling stability comparable to NCM811 cathode (Figure 4d). It demonstrated that the $Li_{1.2}$NCM811 cathode not only can release much more Li in the initial charge but also has a higher capacity with outstanding cycling stability.

It is worth noting that the reason why we prefer anode-free is that Cu foil has a higher Li utilization efficiency over Li foil. The irreversible loss of active Li cycling on Cu foil will be lower than that on Li foil, resulting in higher capacity retention achieving of AF-LMBs. Because the surface of Li foil has unavoidably a passivation layer composed of Li_2O, Li_2CO_3, LiOH, hydrocarbon, and carbonate, leading to a nonuniform lithophilic distribution, negative effecting to the uniform nucleation and growth of Li plating.[18] A similar phenomenon has been studied on Li cycling efficiency on Cu foil and plated Li, proving the advantage of Cu foil.[19] To verify the point, the surface topography images of Cu and Li foils were characterized by Atomic Force Microscopy (AFM). As shown in Figure 5a, Cu foil exhibits a uniform surface, while the surface of Li foil was dispersed with small particles, which is regarded as lithophobic. Thus the wettability of Li foil with electrolyte is worse than that of Cu foil (contact angle: 72.5° VS. 42.7°) (Figure 5b). Then, Cu foil and Li foil paired with Li plates as half-cells, and different amounts of Li were plated onto Cu and Li substrates to observe the different nucleation and growth behaviors of Li. Figures 5c, S17a and S18a show the SEM images of Cu and Li foils after 0.25 mAh cm^{-2} Li plating. As expected, the nucleation of Li on Li substrate is nonuniform. The Li metal first nucleates at high conductive regions and then grow to other regions, laterally grown dendrites. Then, as the amount of Li plating increase to 5 mAh cm^{-2} (Figure 5d, S19a and S20a), all regions of Li substrate are covered by plated Li, but there are still a large number of regions where Li plating is not dense enough, which benefiting the generation of dead Li and the side-reaction of Li with electrolyte.[20] In contrast, Cu foil shows significant advantages over Li foil by providing a uniform Li nucleation (Figure 5c, S17b and S18b) and dense Li

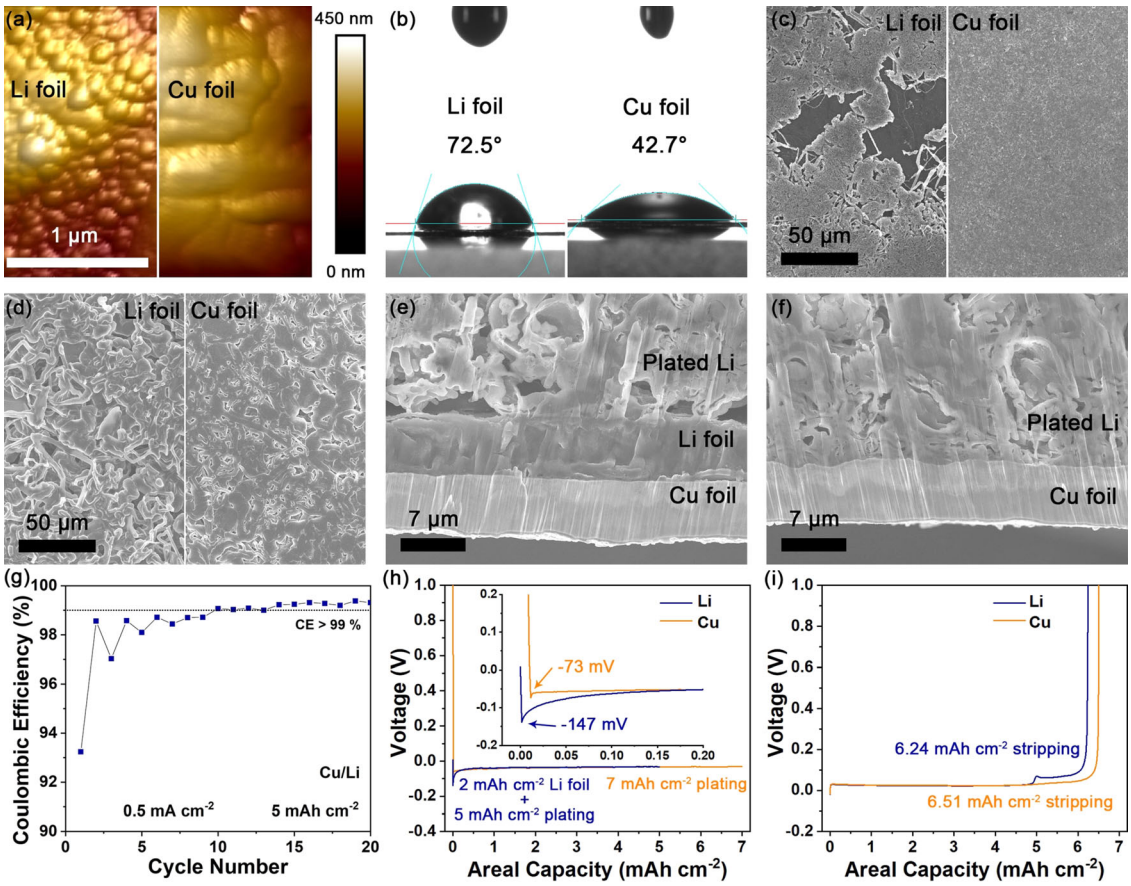

Figure 5. The Li depositing/stripping behavior on Li and Cu substrate. a) Surface topography AFM images of Li foil (left) and Cu foil (right). b) Contact angles of electrolyte on Li foil (left) and Cu foil (right). SEM images of Li foil (left) and Cu foil (right) after c) 0.25 mAh cm^{-2} and d) 5 mAh cm^{-2} Li plating at 0.5 mA cm^{-2}. Cross-section SEM images of e) Li foil and f) Cu foil after 5 mAh cm^{-2} Li plating at 0.5 mA cm^{-2}. g) CE of a Cu/Li half-cell using 6 m LiFSI in DME as the electrolyte. h) Voltage profiles of Li plating onto Li foil and Cu foil for the first cycle with a current density of 0.5 mA cm^{-2}. i) Voltage profiles of Li stripping from Li foil and Cu foil after cycling with a fixed capacity of 5 mAh cm^{-2} for 5 times at 0.5 mA cm^{-2}.

plating morphology (Figure 5d, S19b and S20b). To better understand the nucleation and growth behavior of Li plating, the cross-sections of Cu and Li substrates after Li plating were prepared by Focused Ion Beam (FIB), as shown in Figure 5e, f and S21. Because of the inhomogeneity of Li nucleation, a large number of voids can be observed at the interface between Li substrate and plated Li. Because of the scarcity of nucleation sites, the real current density of Li plating is much higher than the set value, which benefiting the generation of Li dendrites. This highly porous Li plating morphology is also more likely to lead to the formation of isolated "dead Li" during Li stripping, which seriously affects the lifespan of Li anode. While Cu foil shows much denser Li plating morphology, significant advantages than Li foil (Figure 5f and S21b) because the conductivity and lithophilicity distribution on the Cu surface is much more uniform, higher CE of Li plating/stripping in appropriate electrolytes.[8c,9,12j,k,21] Figure 5g shows the CE of a Cu/Li half-cell using 6 m LiFSI in DME (6 mol LiFSI salt in 1 liter DME solvent) as electrolyte under 0.5 mA cm^{-2} and 5 mAh cm^{-2}. The CE of the cell reached 99% after 10 cycles. The average CE of the first 10 cycles can only reach 97.9% because of the low initial CE (ICE, 93.2%), which reminds us that the capacity loss of anode-free batteries mainly comes from the previous cycles. Therefore, the capacity retention of AF-LMBs can be significantly improved by adding a small amount of Li resources to offset the irreversible Li loss in previous cycles. And it is quite important to Figure out whether the extra Li should be added to anode or cathode.

Since Li substrate is less efficient for Li plating, attaching extra Li foil to anode current collector may reduce the utilization efficiency of limited Li resources from cathode materials. To verify this, $Li_{Limited}$/Li cell was assembled by using limited Li foil (2 mAh cm^{-2}) covered Cu foil as a working electrode and Li plate as a counter electrode, while Cu/Li cell was assembled by using Cu foil as a working electrode and Li plate as a counter electrode. In order to ensure the same amount of active Li on both two working electrodes (7 mAh cm^{-2}), 5 mAh cm^{-2} Li was plated onto the limited Li electrode and 7 mAh cm^{-2} Li was plated onto the Cu electrode (Figure 5h). Notably, the plating of Li onto Cu foil exhibits a smaller nucleation overpotential of −73 mV (the inset of Figure 5h), almost half of that on Li foil (−147 mV). Then, 5 mAh cm^{-2} Li in the working electrodes are continuously stripped/plated for 5 times (Figure S22). Finally, these half-cells are charged to 2 V to ensure that the remaining active Li on the working electrodes are completely stripped (Figure 5i). The only difference between these two working electrodes is that Li cycles on Li or Cu substrates, therefore, the amount of residual active Li directly reflects the Li utilization efficiency of these two working electrodes.[22] As expected, Cu electrode shows a higher Li utilization efficiency with 6.51 mAh cm^{-2} residual active Li, when comparing with 6.24 mAh cm^{-2} for limited Li electrode, proving the advantages of Cu substrate over Li. These results highlight the advantage of this strategy by storing extra active Li in cathode material rather than directly attaching it to the anode, especially when the amount of Li added is extremely limited.

Encouraged by the results in the half-cells, the 60 mAh level single-layer anode-free pouch cells are assembled where $Li_{1.37}$NCM811(prepared by electrochemical method, Figure S3) and NCM811 electrodes (25 mg cm^{-2}, 30 × 41 mm^2) paired with Cu foils (31 × 41 mm^2), respectively (Please see the detailed parameters of the pouch cell in Table S4 and S5). Figure 6a shows that the $Li_{1.37}$NCM811/Cu exhibits not only superior cycling stability than NCM811/Cu but also better than the NCM811/Li batteries, where excessive Li (2 mAh cm^{-2}) is applied. Detailedly, $Li_{1.37}$NCM811/Cu outperforms NCM811/Li in initial specific capacity (203 mAh cm^{-2} vs. 194 mAh cm^{-2}) and exhibits capacity retention of 84% after 100 cycles, much higher than that of NCM811/Li (68%) (as shown in Figure 6a). Besides, to evaluate the real energy density of our AF-LMBs, we assembled the hand-made level multi-layer anode-free pouch cells (300 mAh) where $Li_{1.31}$NCM811 (lithiated by n-butyl Li, 31.25 mg cm^{-2}, 30 × 40 mm^2) paired with Cu foil (31 × 41 mm^2) (Figure 6b–d). As shown in Figure 6c, $Li_{1.31}$NCM811/Cu outperforms NCM811/Li in initial energy density (447 Wh kg^{-1} vs. 415 Wh kg^{-1}), and the energy density remains 416 Wh kg^{-1} after 50 cycles. The energy density of this $Li_{1.31}$NCM811/Cu cell is determined from the weight of the cell core, excluding the weight of Al-plastic film packaging (21.8 wt%).[23] Notably, the energy density based on the total weight of a single cell can reach 350 Wh kg^{-1} (Table S6), still one of the highest among reported AF-LMBs (Table S2). Figure 6e shows the first cycle voltage profiles of NCM811/Cu, NCM811/Li, and $Li_{1.37}$NCM811/Cu pouch cells. Compared with the other two cells, a new change plateau appears at 2.4 V in $Li_{1.37}$NCM811/Cu, corresponding to the transfer of active Li from $Li_{1.37}$NCM811 cathode to anode as Li reservoir, resulting in the highest charge capacity of 312 mAh g^{-1}. Figure 6f shows the normalized voltage profiles of $Li_{1.35}$NCM811/Cu pouch cells at the 2nd and 100th cycles. Even after 100 cycles, the working voltage of $Li_{1.35}$NCM811/Cu nearly no drops whose energy efficiency maintained above 94.92% (the 2nd cycle: 95.22%), confirming the stability of battery operation.

Conclusion

In conclusion, we propose to adopt the Li-rich $P\bar{3}m1$ type $Li_2[Ni_{0.8}Co_{0.1}Mn_{0.1}]O_2$ (Li_2NCM811) to configure the anode free Li metal batteries that enable to prolong the lifespan of AF-LMB in the high energy density level. In the first charge process, the Li_2NCM811 cathode not only acted as an extender to release an extra amount of Li-ions that supplements the Li loss in the anode but also reversibly converted back to NCM811, thereby extending the lifespan of the battery without the introduction of inactive elements, like a disposable fuel tank for a space shuttle. Meanwhile, after the lithium releasing process. By the benefit of Li-rich cathode, the anode-free pouch cell enables to achieve the capacity retention above 84% after 100 cycles in the condition of high cathode mass loading (25 mg cm^{-2}) and limited electrolyte addition (E/C ratio of 2 g Ah^{-1}). The energy density of 300 mAh level multi-layer AF-LMB using this Li-rich cath-

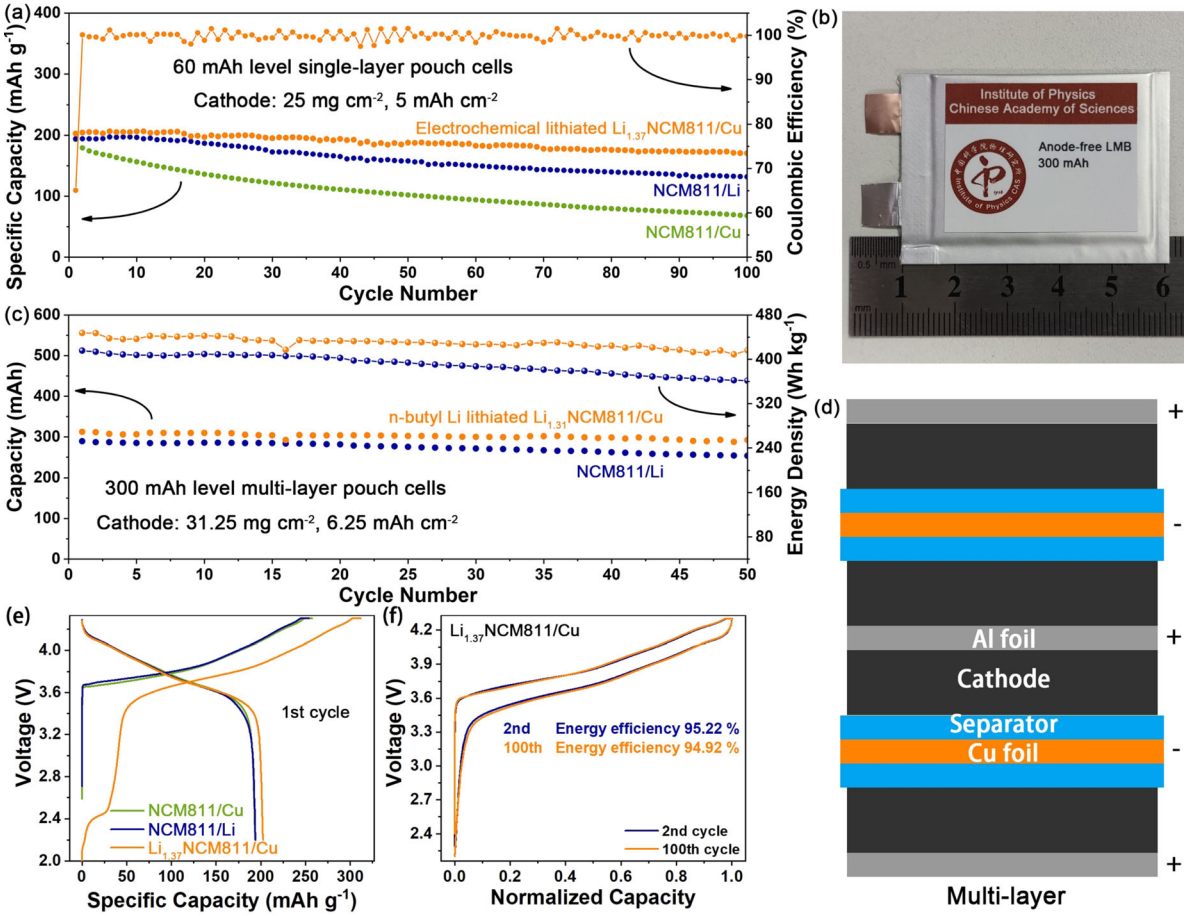

Figure 6. The demonstration of anode-free $Li_{1+x}NCM811$ pouch cells. a) Cycling performances of NCM811/Cu, NCM811/Li, and $Li_{1.37}NCM811/Cu$ pouch cells. b) Picture of 300 mAh level multi-layer anode-free pouch cell. c) Capacity and energy density of multi-layer NCM811/Li and $Li_{1.31}NCM811/Cu$ pouch cells. d) Illustration of multi-layer anode-free pouch cell. e) Voltage profiles of NCM811/Cu, NCM811/Li, and $Li_{1.37}NCM811/Cu$ pouch cells. f) Normalized capacities and corresponding energy efficiencies of $Li_{1.37}NCM811/Cu$ pouch cell at different cycles. ($Li_{1.37}NCM811$ was electrochemical lithiated as illustrated in Figure S3. $Li_{1.31}NCM811$ was lithiated by n-butyl Li. The pouch cells were charged at 0.5 mA cm^{-2} and discharged at 1 mA cm^{-2} with a pressure of 250 kPa.)

ode can achieve 447 Wh kg^{-1}. All these above advantages make this strategy attractive to the further development of high energy density batteries by extending their lifespans.

Acknowledgements

This work is supported by National Key Technologies R&D Program, China (2018YFB0104400), and the Center for Clean Energy. L.L. acknowledges China Postdoctoral Science Foundation (2019M660845).

Conflict of interest

The authors declare no conflict of interest.

Keywords: anode-free · layered compounds · Li-rich cathodes · lithiation · lithium metal batteries

[1] a) M. Armand, J. M. Tarascon, *Nature* **2008**, *451*, 652; b) B. Dunn, H. Kamath, J.-M. Tarascon, *Science* **2011**, *334*, 928; c) J. W. Choi, D. Aurbach, *Nat. Rev. Mater.* **2016**, *1*, 16013.
[2] J. B. Goodenough, Y. Kim, *Chem. Mater.* **2010**, *22*, 587.
[3] a) P. Albertus, S. Babinec, S. Litzelman, A. Newman, *Nat. Energy* **2018**, *3*, 16; b) D. Lin, Y. Liu, Y. Cui, *Nat. Nanotechnol.* **2017**, *12*, 194.
[4] a) J. Qian, B. D. Adams, J. Zheng, W. Xu, W. A. Henderson, J. Wang, M. E. Bowden, S. Xu, J. Hu, J.-G. Zhang, *Adv. Funct. Mater.* **2016**, *26*, 7094; b) R. Weber, M. Genovese, A. J. Louli, S. Hames, C. Martin, I. G. Hill, J. R. Dahn, *Nat. Energy* **2019**, *4*, 683.
[5] S. Nanda, A. Gupta, A. Manthiram, *Adv. Energy Mater.* **2021**, *11*, 2000804.
[6] a) M. S. Whittingham, *Chem. Rev.* **2004**, *104*, 4271; b) A. Nytén, A. Abouimrane, M. Armand, T. Gustafsson, J. O. Thomas, *Electrochem. Commun.* **2005**, *7*, 156; c) T. Ohzuku, *J. Electrochem. Soc.* **1993**, *140*, 1862; d) N. N. Bramnik, K. G. Bramnik, T. Buhrmester, C. Baehtz, H. Ehrenberg, H. Fuess, *J. Solid State Electrochem.* **2004**, *8*, 558; e) C. Liu, Z. G. Neale, G. Cao, *Mater. Today* **2016**, *19*, 109; f) N. Kuwata, S. Kudo, Y. Matsuda, J. Kawamura, *Solid State Ionics* **2014**, *262*, 165.

[7] a) Y.-K. Sun, S.-T. Myung, M.-H. Kim, J. Prakash, K. Amine, *J. Am. Chem. Soc.* **2005**, *127*, 13411; b) M.-H. Kim, H.-S. Shin, D. Shin, Y.-K. Sun, *J. Power Sources* **2006**, *159*, 1328.

[8] a) X. Ren, L. Zou, X. Cao, M. H. Engelhard, W. Liu, S. D. Burton, H. Lee, C. Niu, B. E. Matthews, Z. Zhu, C. Wang, B. W. Arey, J. Xiao, J. Liu, J.-G. Zhang, W. Xu, *Joule* **2019**, *3*, 1662; b) X. Cao, X. Ren, L. Zou, M. H. Engelhard, W. Huang, H. Wang, B. E. Matthews, H. Lee, C. Niu, B. W. Arey, Y. Cui, C. Wang, J. Xiao, J. Liu, W. Xu, J.-G. Zhang, *Nat. Energy* **2019**, *4*, 796; c) X. Fan, L. Chen, O. Borodin, X. Ji, J. Chen, S. Hou, T. Deng, J. Zheng, C. Yang, S.-C. Liou, K. Amine, K. Xu, C. Wang, *Nat. Nanotechnol.* **2018**, *13*, 715; d) C. Niu, H. Pan, W. Xu, J. Xiao, J.-G. Zhang, L. Luo, C. Wang, D. Mei, J. Meng, X. Wang, Z. Liu, L. Mai, J. Liu, *Nat. Nanotechnol.* **2019**, *14*, 594.

[9] a) S. Chen, J. Zheng, D. Mei, K. S. Han, M. H. Engelhard, W. Zhao, W. Xu, J. Liu, J.-G. Zhang, *Adv. Mater.* **2018**, *30*, 1706102; b) Y. Yang, D. M. Davies, Y. Yin, O. Borodin, J. Z. Lee, C. Fang, M. Olguin, Y. Zhang, E. S. Sablina, X. Wang, C. S. Rustomji, Y. S. Meng, *Joule* **2019**, *3*, 1986; c) L. Suo, W. Xue, M. Gobet, S. G. Greenbaum, C. Wang, Y. Chen, W. Yang, Y. Li, J. Li, *Proc. Natl. Acad. Sci. USA* **2018**, *115*, 1156.

[10] C. Yan, H.-R. Li, X. Chen, X.-Q. Zhang, X.-B. Cheng, R. Xu, J.-Q. Huang, Q. Zhang, *J. Am. Chem. Soc.* **2019**, *141*, 9422.

[11] K.-H. Chen, A. J. Sanchez, E. Kazyak, A. L. Davis, N. P. Dasgupta, *Adv. Energy Mater.* **2019**, *9*, 1802534.

[12] a) T. T. Hagos, B. Thirumalraj, C. J. Huang, L. H. Abrha, T. M. Hagos, G. B. Berhe, H. K. Bezabh, J. Cherng, S. F. Chiu, W. N. Su, B. J. Hwang, *ACS Appl. Mater. Interfaces* **2019**, *11*, 9955; b) L. H. Abrha, T. A. Zegeye, T. T. Hagos, H. Sutiono, T. M. Hagos, G. B. Berhe, C. J. Huang, S. K. Jiang, W. N. Su, Y. W. Yang, B. J. Hwang, *Electrochim. Acta* **2019**, *325*, 134825; c) T. M. Hagos, G. B. Berhe, T. T. Hagos, H. K. Bezabh, L. H. Abrha, T. T. Beyene, C.-J. Huang, Y.-W. Yang, W.-N. Su, H. Dai, B.-J. Hwang, *Electrochim. Acta* **2019**, *316*, 52; d) S. S. Zhang, X. L. Fan, C. S. Wang, *Electrochim. Acta* **2017**, *258*, 1201; e) J. Alvarado, M. A. Schroeder, T. P. Pollard, X. Wang, J. Z. Lee, M. Zhang, T. Wynn, M. Ding, O. Borodin, Y. S. Meng, K. Xu, *Energy Environ. Sci.* **2019**, *12*, 780; f) M. Genovese, A. J. Louli, R. Weber, C. Martin, T. Taskovic, J. R. Dahn, *J. Electrochem. Soc.* **2019**, *166*, A3342; g) A. J. Louli, M. Genovese, R. Weber, S. G. Hames, E. R. Logan, J. R. Dahn, *J. Electrochem. Soc.* **2019**, *166*, A1291; h) N. A. Sahalie, A. A. Assegie, W. N. Su, Z. T. Wondimkun, B. A. Jote, B. Thirumalraj, C. J. Huang, Y. W. Yang, B. J. Hwang, *J. Power Sources* **2019**, *437*, 226912; i) Z. T. Wondimkun, T. T. Beyene, M. A. Weret, N. A. Sahalie, C. J. Huang, B. Thirumalraj, B. A. Jote, D. Y. Wang, W. N. Su, C. H. Wang, G. Brunklaus, M. Winter, B. J. Hwang, *J. Power Sources* **2020**, *450*, 227589; j) A. J. Louli, A. Eldesoky, R. Weber, M. Genovese, M. Coon, J. deGooyer, Z. Deng, R. T. White, J. Lee, T. Rodgers, R. Petibon, S. Hy, S. J. H. Cheng, J. R. Dahn, *Nat. Energy* **2020**, *5*, 693; k) Z. Yu, H. Wang, X. Kong, W. Huang, Y. Tsao, D. G. Mackanic, K. Wang, X. Wang, W. Huang, S. Choudhury, Y. Zheng, C. V. Amanchukwu, S. T. Hung, Y. Ma, E. G. Lomeli, J. Qin, Y. Cui, Z. Bao, *Nat. Energy* **2020**, *5*, 526.

[13] a) C. Ghanty, B. Markovsky, E. M. Erickson, M. Talianker, O. Haik, Y. Tal-Yossef, A. Mor, D. Aurbach, J. Lampert, A. Volkov, J.-Y. Shin, A. Garsuch, F. F. Chesneau, C. Erk, *ChemElectroChem* **2015**, *2*, 1479; b) J. Cho, T.-J. Kim, J. Kim, M. Noh, B. Park, *J. Electrochem. Soc.* **2004**, *151*, A1899; c) A. O. Kondrakov, A. Schmidt, J. Xu, H. Geßwein, R. Mönig, P. Hartmann, H. Sommer, T. Brezesinski, J. Janek, *J. Phys. Chem. C* **2017**, *121*, 3286; d) Y. Bi, W. Yang, R. Du, J. Zhou, M. Liu, Y. Liu, D. Wang, *J. Power Sources* **2015**, *283*, 211.

[14] a) H. Li, G. Richter, J. Maier, *Adv. Mater.* **2003**, *15*, 736; b) H. Lee, S.-K. Chang, E.-Y. Goh, J.-Y. Jeong, J. H. Lee, H.-J. Kim, J.-J. Cho, S.-T. Hong, *Chem. Mater.* **2008**, *20*, 5; c) D. Shanmukaraj, S. Grugeon, S. Laruelle, G. Douglade, J.-M. Tarascon, M. Armand, *Electrochem. Commun.* **2010**, *12*, 1344; d) M. G. Kim, J. Cho, *J. Mater. Chem.* **2008**, *18*, 5880; e) X. Su, C. Lin, X. Wang, V. A. Maroni, Y. Ren, C. S. Johnson, W. Lu, *J. Power Sources* **2016**, *324*, 150; f) J. Du, W. Wang, A. Y. Sheng Eng, X. Liu, M. Wan, Z. W. Seh, Y. Sun, *Nano Lett.* **2020**, *20*, 546; g) J. Zhao, Z. Lu, N. Liu, H.-W. Lee, M. T. McDowell, Y. Cui, *Nat. Commun.* **2014**, *5*, 5088; h) P. Poizot, S. Laruelle, S. Grugeon, L. Dupont, J. M. Tarascon, *Nature* **2000**, *407*, 496.

[15] a) M. Bianchini, M. Roca-Ayats, P. Hartmann, T. Brezesinski, J. Janek, *Angew. Chem. Int. Ed.* **2019**, *58*, 10434; *Angew. Chem.* **2019**, *131*, 10542; b) K. Kang, C.-H. Chen, B. J. Hwang, G. Ceder, *Chem. Mater.* **2004**, *16*, 2685.

[16] a) J. R. Dahn, U. von Sacken, C. A. Michal, *Solid State Ionics* **1990**, *44*, 87; b) I. Davidson, J. E. Greedan, U. von Sacken, C. A. Michal, J. R. Dahn, *Solid State Ionics* **1991**, *46*, 243.

[17] D. Zhou, Y. Jia, X. Duan, J. Tang, J. Xu, D. Liu, X. Xiong, J. Zhang, J. Luo, L. Zheng, B. Liu, Y. Kuang, X. Sun, X. Duan, *Nano Energy* **2019**, *60*, 661.

[18] a) H. Chen, A. Pei, D. Lin, J. Xie, A. Yang, J. Xu, K. Lin, J. Wang, H. Wang, D. Boyle, Y. Cui, *Adv. Energy Mater.* **2019**, *9*, 1900858; b) N. Li, Y. Yin, C. Yang, Y. Guo, *Adv. Mater.* **2016**, *28*, 1853; c) K. Kanamura, *J. Electrochem. Soc.* **1995**, *142*, 340; d) D. Lin, Y. Liu, W. Chen, G. Zhou, K. Liu, B. Dunn, Y. Cui, *Nano Lett.* **2017**, *17*, 3731.

[19] M. Genovese, A. J. Louli, R. Weber, S. Hames, J. R. Dahn, *J. Electrochem. Soc.* **2018**, *165*, A3321.

[20] a) S. Li, M. Jiang, Y. Xie, H. Xu, J. Jia, J. Li, *Adv. Mater.* **2018**, *30*, 1706375; b) A. Kushima, K. P. So, C. Su, P. Bai, N. Kuriyama, T. Maebashi, Y. Fujiwara, M. Z. Bazant, J. Li, *Nano Energy* **2017**, *32*, 271; c) C. Fang, J. Li, M. Zhang, Y. Zhang, F. Yang, J. Z. Lee, M.-H. Lee, J. Alvarado, M. A. Schroeder, Y. Yang, B. Lu, N. Williams, M. Ceja, L. Yang, M. Cai, J. Gu, K. Xu, X. Wang, Y. S. Meng, *Nature* **2019**, *572*, 511.

[21] a) X. Fan, L. Chen, X. Ji, T. Deng, S. Hou, J. Chen, J. Zheng, F. Wang, J. Jiang, K. Xu, C. Wang, *Chem* **2018**, *4*, 174; b) X. Ren, S. Chen, H. Lee, D. Mei, M. H. Engelhard, S. D. Burton, W. Zhao, J. Zheng, Q. Li, M. S. Ding, M. Schroeder, J. Alvarado, K. Xu, Y. S. Meng, J. Liu, J.-G. Zhang, W. Xu, *Chem* **2018**, *4*, 1877; c) S. Chen, J. Zheng, L. Yu, X. Ren, M. H. Engelhard, C. Niu, H. Lee, W. Xu, J. Xiao, J. Liu, J.-G. Zhang, *Joule* **2018**, *2*, 1548; d) W. Li, H. Yao, K. Yan, G. Zheng, Z. Liang, Y.-M. Chiang, Y. Cui, *Nat. Commun.* **2015**, *6*, 7436.

[22] B. D. Adams, J. Zheng, X. Ren, W. Xu, J.-G. Zhang, *Adv. Energy Mater.* **2018**, *8*, 1702097.

[23] J. Betz, G. Bieker, P. Meister, T. Placke, M. Winter, R. Schmuch, *Adv. Energy Mater.* **2019**, *9*, 1803170.

Manuscript received: December 23, 2020
Accepted manuscript online: January 25, 2021
Version of record online: ■■ ■■, ■■■■

Research Articles

Lithium Metal Batteries

L. Lin, K. Qin, Q. Zhang, L. Gu, L. Suo,* Y. Hu, H. Li, X. Huang, L. Chen ———— ▮▮▮▮–▮▮▮▮

Li-Rich $Li_2[Ni_{0.8}Co_{0.1}Mn_{0.1}]O_2$ for Anode-Free Lithium Metal Batteries

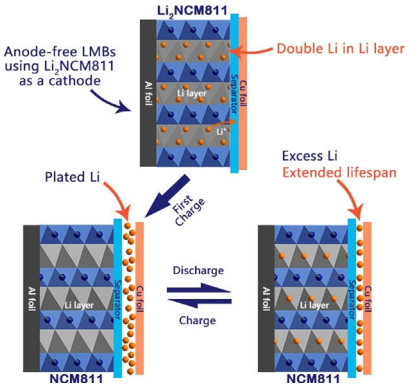

Li-rich $Li_2[Ni_{0.8}Co_{0.1}Mn_{0.1}]O_2$ (Li_2NCM811) contains twice as much Li as NCM811 and can be converted into NCM811 by de-intercalation of Li-ions. When applied in anode-free lithium metal batteries, Li_2NCM811 can release a large amount of Li-ions during the first charging process to supplement the Li loss in the anode, then convert into NCM811, thus extending the lifespan of the battery without the introduction of inactive elements.